Available online at www.sciencedirect.com
ScienceDirect
International Journal of Solids and Structures 45 (2008) 2220–2232
INTERNATIONAL JOURNAL OF SOLIDS AND STRUCTURES
www.elsevier.com/locate/ijsolstr

Effects of thickness on the largely-deformed JKR (Johnson–Kendall–Roberts) test of soft elastic layers

Yu-Yun Lin *, Chun-Fu Chang, Wei-Te Lee

Department of Civil Engineering, National Cheng Kung University, Tainan 70101, Taiwan

Received 31 August 2007; received in revised form 7 November 2007
Available online 15 December 2007

Abstract

The paper aimed to study the effect of large deformation and material nonlinearity on the adhesive contact between a smooth rigid spherical indenter and a Neo-Hookean layer of finite thickness, for the cases of the layer thickness/indenter radius ratio between 1 and 2. Our analysis was based on the large-deformation JKR (LDJKR) theory, which models the adhesive contact of two elastic solids in large-deformation regime by knowing the solution of the corresponding non-adhesive contact problem. In this paper, the non-adhesive contact between a spherical indenter and a Neo-Hookean layer was solved by finite element analysis. Combined these numerical results and the LDJKR theory, approximate analytic expressions of the applied load and displacement of adhesive contact of Neo-Hookean layers were obtained. The effects of layer thickness were also discussed.

Keywords: JKR test; Adhesive contact; Large deformation

1. Introduction

The contact test based on JKR (Johnson–Kendall–Roberts) theory of adhesion (Johnson et al., 1971) has widely used in quantifying the work of adhesion between two soft elastic materials (Chaudhury and Whitesides, 1991; Ahn and Shull, 1998; Ghatak et al., 2000; Maugis and Barquins, 1978; Shull, 2002). This theory is applicable when the contact radius is small in comparison with the radius of the spheres. For example, it cannot be applied to thin elastic lenses. Extension of the JKR theory to handle thin lenses has been addressed by Shull et al. (1998). However, it should be noted that JKR theory assumes small strains and material linearity (Hui et al., 2000). There are many problems of practical interest where these conditions are not satisfied. For example, the elastic modulus of elastic gels and pressure sensitive adhesives can be lower than 10^4 Pa, specimens made of these materials can undergo very large deformation during a JKR test. The same issues are present in adhesive contact of a micro- or nano-indenters on thin and compliant coatings. Barthel and Par-

* Corresponding author. Tel.: +886 6 2757575x63129; fax: +886 6 2358542.
E-mail address: cyylin@mail.ncku.edu.tw (Y.-Y. Lin).

0020-7683/$ - see front matter © 2007 Elsevier Ltd. All rights reserved.
doi:10.1016/j.ijsolstr.2007.11.025

riot (2007) analyzed the adhesive contact of a coated elastic substrate. In these problems, the radii of the indenters are typically on the same order of the substrate. So far, most of the analyses were carried out using small strain theory (Barthel and Parriot, 2007; Yang, 2003a,b; Reedy, 2006). Therefore, it is important to study the applicability of the small strain JKR theory in the large-deformation regime.

When the contact radius is not small in comparison with the radius of spheres, the Hertz assumption of replacing the spheres by an infinite half space is no longer valid. In addition, since the deformation is large, the strains do not depend linearly on the displacement gradients; and the constitutive model relating the deformation to the stress field is no longer linear. Consequently, the stress field can no longer be obtained by superimposing the singular stress field caused by adhesion to the non-adhesive Hertz stress field. Lin and Chen (2006) developed a theory which models large-deformation adhesive contact of hyperelastic lenses based on energy balance. They calculated the energy release rate of a large-deformation JKR (LDJKR) problem using the solution of the corresponding large-deformation Hertz (LDH) problem. Two problems were studied in their work (Lin and Chen, 2006) a rigid spherical indenter in contact with a Neo-Hookean half space, and a Neo-Hookean hemisphere in contact with a rigid substrate. In this paper we extend this work to the case of a compliant layer.

2. Theoretical background

In this section we briefly summarized the large-deformation JKR theory (LDJKR) developed by Lin and Chen (2006) for the adhesive contact of two hyperelastic solid lenses. This theory is an extension of the derivation by Shull et al. (1998) to the large-deformation regime. The geometry is shown schematically in Fig. 1. The thicknesses of these lenses are denoted by h_1 and h_2, respectively. Let a, P, $\delta = \delta_1 + \delta_2$, denote the current projected contact radius, the current load, and total applied displacements, respectively. The air gap outside the contact region can be viewed as an external crack. A fundamental quantity in JKR theory is the energy release rate G of this crack as a function of and the material properties. It should be noted that since the criterion for bonding and debonding is not specified, a, δ must be considered as independent variables. Let denote the current projected contact area. The energy release rate, in a displacement control test, is

$$G = \left.\frac{\partial U_{SE}}{\partial A}\right|_{\delta}, \tag{1}$$

where $U_{SE} = U_{SE}(a,\delta)$ is the elastic strain energy of the system. To compute G, Lin and Chen (2006) divided the loading into two stages. In the first stage (Hertz), the adhesive force is turned off and the lenses are loaded until the projected contact area reaches A. The external load and the displacement in the first stage are denoted by P_H and δ_H, respectively. In the second, the projected contact area A is fixed and the adhesive forces are turned on. Due to adhesion, the external load P must decrease in the second stage. The external load and the displacement at the end of this process is the actual load and displacement, P and δ, respectively. Since the deformation during the second stage is typically small,

$$\frac{\delta - \delta_H(a)}{P - P_H(a)} \simeq C_H(a) = \left.\frac{\partial \delta_H}{\partial P_H}\right|_{a}. \tag{2}$$

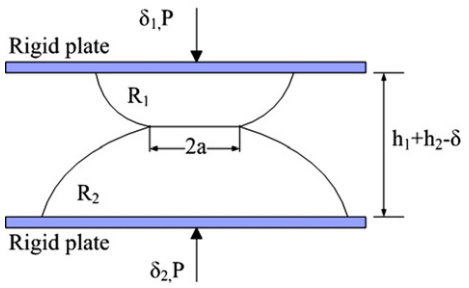

Fig. 1. Illustration of JKR test of two lenses.

The energy release rate can be simplified and results in

$$G = -\frac{C'_{\mathrm{H}}(a)}{4\pi a}\left(\frac{\delta - \delta_{\mathrm{H}}(a)}{C_{\mathrm{H}}(a)}\right)^2, \tag{3}$$

where $C'_{\mathrm{H}}(a) = \mathrm{d}C_{\mathrm{H}}/\mathrm{d}a$. The energy release rate for a load controlled test is obtained using a similar procedure. It is

$$G = -\frac{C'_{\mathrm{H}}(a)}{4\pi a}(P - P_{\mathrm{H}}(a))^2. \tag{4}$$

As a consequence of Eqs. (3) and (4), the energy release rate is determined by the solution of the large-deformation Hertz problem, i.e., P_{H}, δ_{H} and C_{H}.

The large-deformation JKR theory can be obtained by relating the energy release rate in (3) and (4) to the work of adhesion, W. Consider the work of adhesion W be the energy to adhere a unit of true surface area A', where $A' = 2\pi R^2\left[1 - \sqrt{1 - \left(\frac{a}{R}\right)^2}\right]$. Hence, $W = \frac{\mathrm{d}U}{\mathrm{d}A'} = \frac{\mathrm{d}U}{\mathrm{d}A}\frac{\mathrm{d}A}{\mathrm{d}A'} = G\sqrt{1 - \left(\frac{a}{R}\right)^2}$. Substituting this relation into (3) and (4), we obtained

$$\delta = \delta_{\mathrm{H}}(a) - C_{\mathrm{H}}(a)\sqrt{\frac{-4\pi a W\left[1 - \left(\frac{a}{R}\right)^2\right]^{-1/2}}{C'_{\mathrm{H}}(a)}}, \tag{5}$$

$$P = P_{\mathrm{H}}(a) - \sqrt{\frac{-4\pi a W\left[1 - \left(\frac{a}{R}\right)^2\right]^{-1/2}}{C'_{\mathrm{H}}(a)}}. \tag{6}$$

Eqs. (5) and (6) have the same form as the standard JKR theory for small a/R, except that P_{H}, and δ_{H} are the large-deformation Hertz load and displacement and C_{H} is the large-deformation Hertz compliance.

3. Geometry, material and normalization

We consider a smooth rigid spherical indenter of radius R in contact with a Neo-Hookean layer of thickness h as shown in Fig. 2. The bottom of the elastic layer is assumed to be perfectly bonded to a rigid substrate. The interface between the sphere and the elastic layer is assumed to be frictionless. The material is modeled as an incompressible Neo-Hookean solid. The strain energy density Φ is

$$\Phi = \frac{\mu}{2}(I_1 - 3), \tag{7}$$

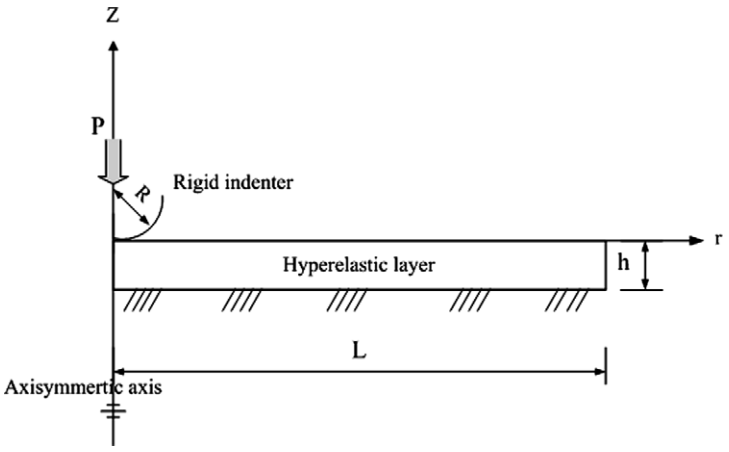

Fig. 2. A spherical rigid indenter contacts on a hyperelastic layer. Top surface of the layer is assumed frictionless and the bottom surface is assumed fixed.

where μ is the infinitesimal shear modulus and I_1 is an invariant of Cauchy–Green strain tensor, i.e., $I_1 = \sum_{k=1}^{3} \lambda_k^2$, where λ_k is the principal stretch ratio in the kth direction. In simple tension, the Cauchy stress $\sigma \equiv \sigma_{11}$ is related to the $\lambda \equiv \lambda_1$ by

$$\sigma = \mu(\lambda^2 - \lambda^{-1}). \tag{8}$$

According to (5) and (6), the LDJKR solution is completely determined by the dependence of the Hertz load P_H, displacement δ_H and compliance on the contact radius a and specimen geometry. From dimensional considerations,

$$P_H = P_o \phi_1(a/R, h/R), \tag{9}$$

$$\delta_H = \delta_o \phi_2(a/R, h/R), \tag{10}$$

$$C_H = C_o \phi_3(a/R, h/R), \tag{11}$$

respectively, where $P_o = \frac{16\mu a^3}{3R}$, $\delta_o = \frac{a^2}{R}$ and $C_o = \frac{1}{8\mu a}$ are the small strain Hertz load, Hertz displacement and Hertz compliance for a rigid sphere in contact with an incompressible isotropic elastic half space. The dimensionless functions ϕ_1, ϕ_2, ϕ_3 are unknowns and will be determined using finite element method. For small contact, $\phi_1 \to 1$, $\phi_2 \to 1$, $\phi_3 \to 1$, that is, we recover the small strain Hertz theory.

4. Finite element model

As explained above, the key is to determine the compliance of the sample as a function of contact radius. The finite element model is illustrated in Fig. 3. Frictionless condition was applied inside the contact zone and was prescribed on the two surfaces in contact in our finite element model. A typical mesh using axis-symmetric elements CAX4H is shown in Fig. 3. A large number of elements are used near the contact edge for accurate prediction of the contact region. To reach the required accuracy (see discussion below), different meshes will be used for different range of contact radius.

Since the contact area is less sensitive to load variations than displacement variations, the compliance C_H is computed using the following scheme. Let the contact radius, the displacement and the load in the beginning of the kth step be denoted by,and P_k, respectively, $k = 1, 2, \ldots$ Increase the load P_k by a very small amount ΔP_k so that contact radius a_k remains fixed within the accuracy imposed by the finite element mesh. In practice, this condition is satisfied when $\Delta P_k < 0.001 P_k$. Denote the increase in displacement due to this load increment by $\Delta\delta_k$. The compliance at is computed using

$$C_H(a_k) = \frac{\Delta\delta_k}{\Delta P_k}. \tag{12}$$

In the next step, increase the load to P_{k+1} (the step size here is much larger than ΔP_k) to create a new contact radius a_{k+1} and a new displacement δ_{k+1}. The process is repeated until the desired contact radius is reached.

5. FEM results of non-adhesive contact

Finite element results for various thicknesses to radius ratio are presented in Figs. 4–8. Simulations are carried out for $h/R = 1.0$, 1.2, 1.5, 1.8, and 2.0 to very large deformation, with contact area almost equal to the

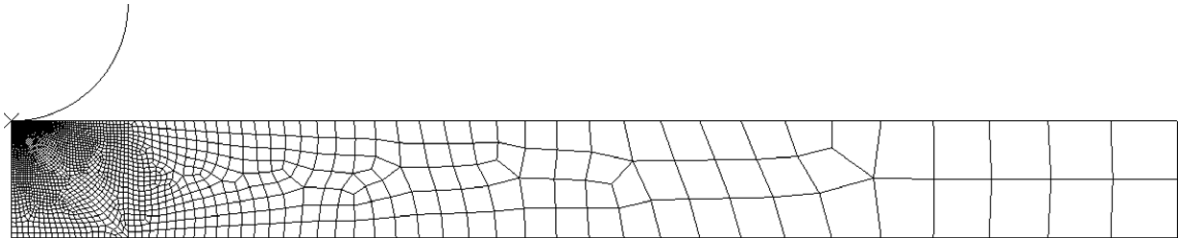

Fig. 3. Typical mesh of non-adhesive contact of a spherical indenter and a hyperelastic layer.

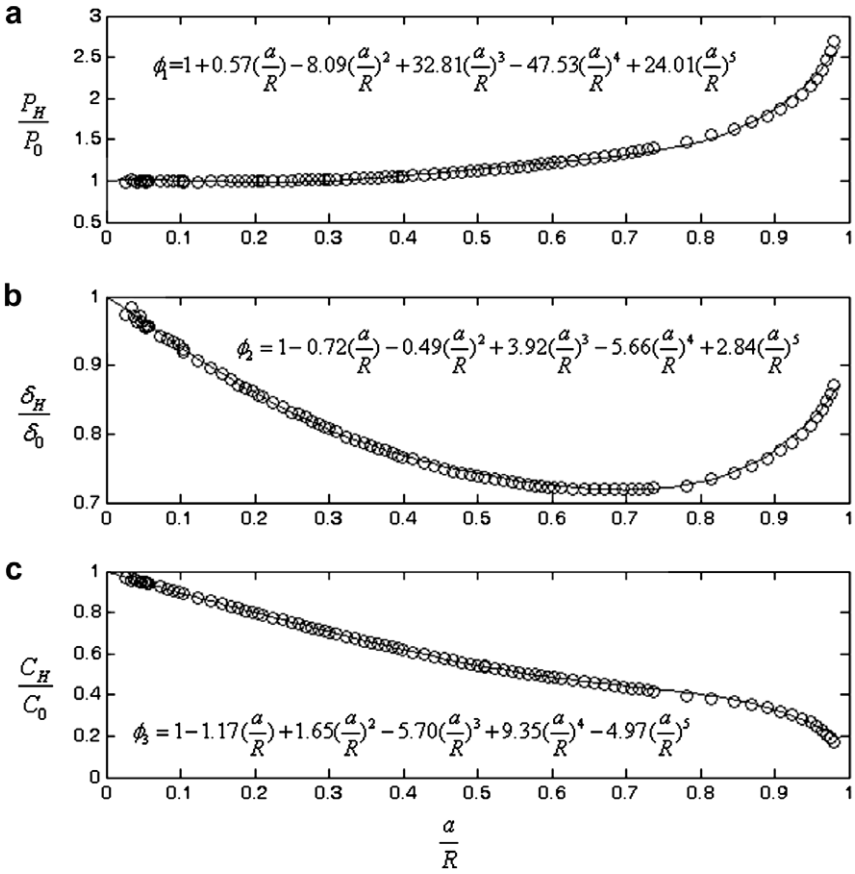

Fig. 4. For $h/R = 1.0$, (a) FEM results (○) of P_H/P_o versus a/R and its fitting function ϕ_1 (solid line) (b) FEM results (○) of δ_H/δ_o versus a/R and its fitting function ϕ_2 (solid line) (c) FEM results (○) of C_H/C_o versus a/R and its fitting function ϕ_3 (solid line).

indenter radius. Each figure consists of three parts, e.g. Fig. 4(a)–(c). The first part (a) in these figures plots the normalized Hertz load, $P_H/P_o = \phi_1$ versus the normalized contact radius, a/R. The second part (b) plots the normalized Hertz displacement $\delta_H/\delta_o = \phi_2$ versus a/R. The last part (c) plots the normalized compliance C_H/C_o versus a/R. Finite element results are denoted by the symbol ○ in these figures. These finite element results are fitted using polynomial functions. The fits are shown in the same figure as solid lines. Equations used for fitting are given in each figure. These equations are very accurate through the entire range of $0 \leqslant a/R < 1$.

Figs. 4(a)–8(a) show that P_H/P_o is greater than 1 for sufficiently large contact, i.e., $0.4 < a/R < 1$. This result shows that the small strain Hertz theory underestimates the actual Hertz load. Also, the thinner the elastic layer, the larger is the deviation. It is surprising that the small strain Hertz load agrees well with the large-deformation Hertz load for contact radius up to 40% of the indenter radius. A different trend is found for displacements. Figs. 4(b)–8(b) show that significant deviation occurs at small contact radius; this is to be expected, as the Hertz displacement used in the normalization do not take into account of the effect of finite layer. For all cases of h/R, the small strain theory overestimates the displacement at small and medium contact. However, for $h/R \geqslant 1.5$, the small strain theory underestimates the displacement for very large contact, as can be seen in Figs. 6(a)–8(a). Note that this effect does not occur for thinner layers. For layers thinner than 1.5R, the small strain Hertz theory overestimates the displacement in the entire range of contact. Finally, the compliance predicted by the small strain theory overestimates the actual compliance in all cases. This is to be expected, since the small strain theory is based on the solution of a rigid punch indenting on a half space.

The fitting functions given in Figs. 4–8 are valid for a specific h/R. It is possible to obtain expressions that work for the entire range of h/R, i.e., $1 \leqslant h/R \leqslant 2$. These functions are found to be

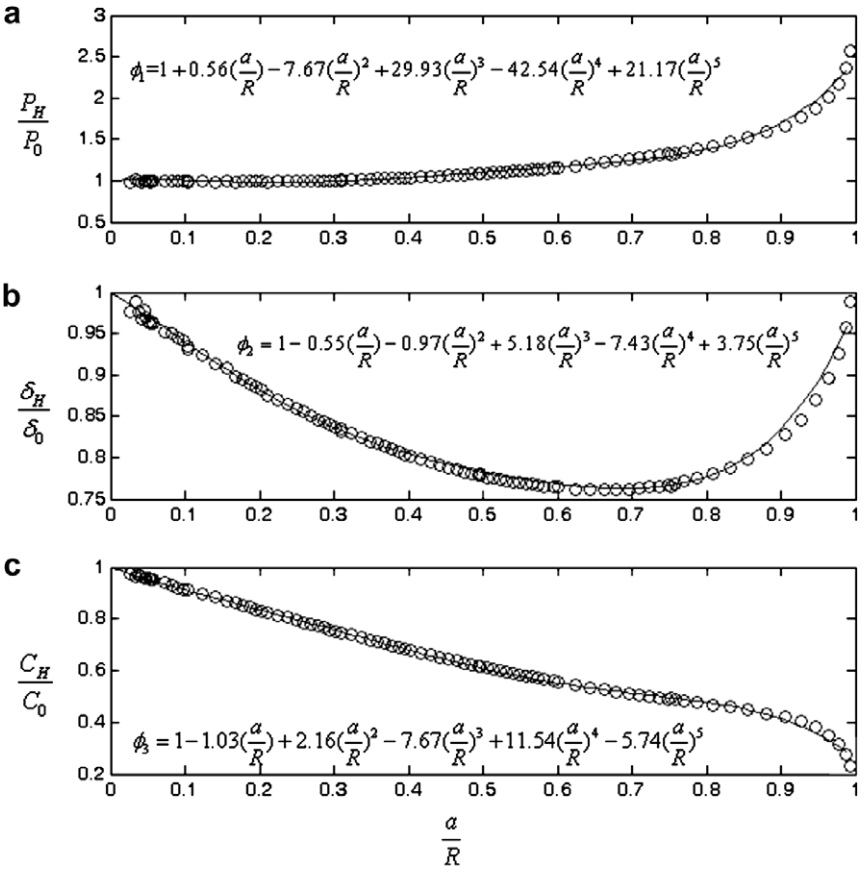

Fig. 5. For $h/R = 1.2$, (a) FEM results (○) of P_H/P_o versus a/R and its fitting function ϕ_1 (solid line) (b) FEM results (○) of δ_H/δ_o versus a/R and its fitting function ϕ_2 (solid line) (c) FEM results (○) of C_H/C_o versus a/R and its fitting function ϕ_3 (solid line).

$$\phi_1\left(\frac{a}{R},\frac{h}{R}\right) = 1 + b_1\left(\frac{a}{R}\right) + b_2\left(\frac{a}{R}\right)^2 + b_3\left(\frac{a}{R}\right)^3 + b_4\left(\frac{a}{R}\right)^4 + b_5\left(\frac{a}{R}\right)^5, \tag{13}$$

$$\phi_2\left(\frac{a}{R},\frac{h}{R}\right) = 1 + c_1\left(\frac{a}{R}\right) + c_2\left(\frac{a}{R}\right)^2 + c_3\left(\frac{a}{R}\right)^3 + c_4\left(\frac{a}{R}\right)^4 + c_5\left(\frac{a}{R}\right)^5, \tag{14}$$

$$\phi_3\left(\frac{a}{R},\frac{h}{R}\right) = 1 + d_1\left(\frac{a}{R}\right) + d_2\left(\frac{a}{R}\right)^2 + d_3\left(\frac{a}{R}\right)^3 + d_4\left(\frac{a}{R}\right)^4 + d_5\left(\frac{a}{R}\right)^5. \tag{15}$$

The coefficients b_i, c_i and d_i in Eqs. (13)–(15) are now functions of normalized the thickness h/R. For $1 \leqslant h/R \leqslant 2$, the coefficients b_i in ϕ_1 are

$$b_1\left(\frac{h}{R}\right) = 30.16 - 89.63\left(\frac{h}{R}\right) + 99.74\left(\frac{h}{R}\right)^2 - 48.19\left(\frac{h}{R}\right)^3 + 8.49\left(\frac{h}{R}\right)^4, \tag{16}$$

$$b_2\left(\frac{h}{R}\right) = -322.97 + 950.03\left(\frac{h}{R}\right) - 1055.02\left(\frac{h}{R}\right)^2 + 509.71\left(\frac{h}{R}\right)^3 - 89.83\left(\frac{h}{R}\right)^4, \tag{17}$$

$$b_3\left(\frac{h}{R}\right) = 1157.2 - 3364.8\left(\frac{h}{R}\right) + 3714\left(\frac{h}{R}\right)^2 - 1788.1\left(\frac{h}{R}\right)^3 + 314.5\left(\frac{h}{R}\right)^4, \tag{18}$$

$$b_4\left(\frac{h}{R}\right) = -1621.3 + 4688.2\left(\frac{h}{R}\right) - 5156.4\left(\frac{h}{R}\right)^2 + 2477\left(\frac{h}{R}\right)^3 - 435.1\left(\frac{h}{R}\right)^4, \tag{19}$$

$$b_5\left(\frac{h}{R}\right) = 777.3 - 2234.8\left(\frac{h}{R}\right) + 2450.3\left(\frac{h}{R}\right)^2 - 1174.9\left(\frac{h}{R}\right)^3 + 206.1\left(\frac{h}{R}\right)^4. \tag{20}$$

The coefficients c_i in ϕ_2 for $1 \leqslant h/R \leqslant 2$ are

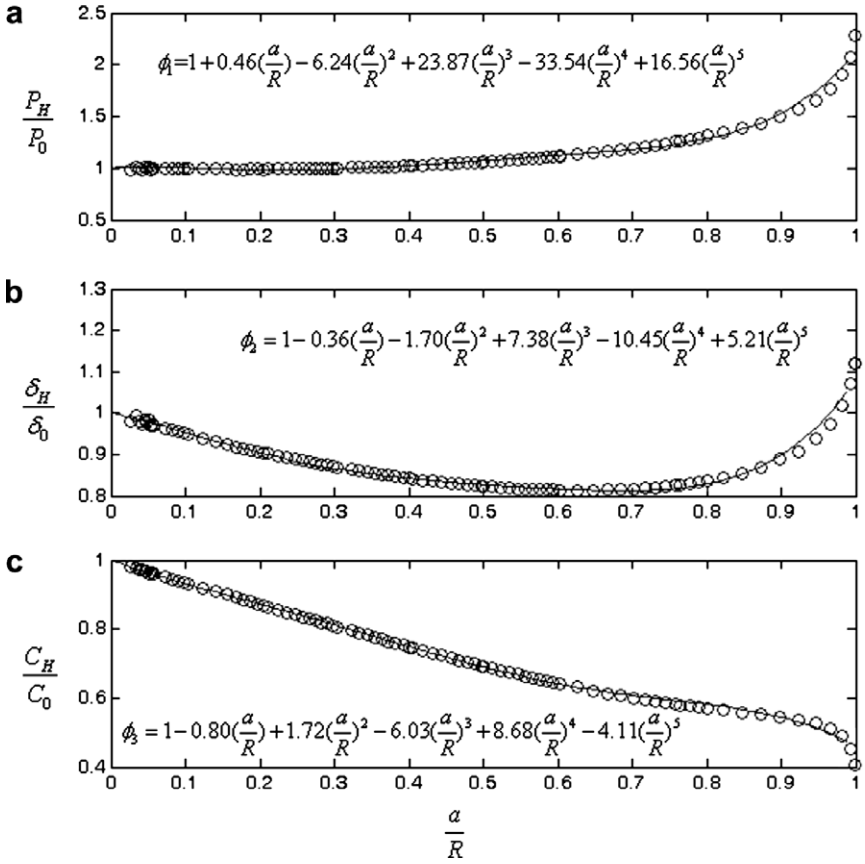

Fig. 6. For $h/R = 1.5$, (a) FEM results (○) of P_H/P_o versus a/R and its fitting function ϕ_1 (solid line) (b) FEM results (○) of δ_H/δ_o versus a/R and its fitting function ϕ_2 (solid line) (c) FEM results (○) of C_H/C_o versus a/R and its fitting function ϕ_3 (solid line).

$$c_1\left(\frac{h}{R}\right) = 11.03 - 37.38\left(\frac{h}{R}\right) + 42.48\left(\frac{h}{R}\right)^2 - 20.40\left(\frac{h}{R}\right)^3 + 3.54\left(\frac{h}{R}\right)^4, \tag{21}$$

$$c_2\left(\frac{h}{R}\right) = -160.42 + 480.37\left(\frac{h}{R}\right) - 526.08\left(\frac{h}{R}\right)^2 + 248.42\left(\frac{h}{R}\right)^3 - 42.78\left(\frac{h}{R}\right)^4, \tag{22}$$

$$c_3\left(\frac{h}{R}\right) = 586.84 - 1744.9\left(\frac{h}{R}\right) + 1907.6\left(\frac{h}{R}\right)^2 - 901.06\left(\frac{h}{R}\right)^3 + 155.43\left(\frac{h}{R}\right)^4, \tag{23}$$

$$c_4\left(\frac{h}{R}\right) = -776.6 + 2308\left(\frac{h}{R}\right) - 2522.7\left(\frac{h}{R}\right)^2 + 1190.8\left(\frac{h}{R}\right)^3 - 205.2\left(\frac{h}{R}\right)^4, \tag{24}$$

$$c_5\left(\frac{h}{R}\right) = 362.4 - 1078.5\left(\frac{h}{R}\right) + 1180.6\left(\frac{h}{R}\right)^2 - 557.94\left(\frac{h}{R}\right)^3 + 96.24\left(\frac{h}{R}\right)^4. \tag{25}$$

The coefficients d_i in ϕ_3 for $1 \leqslant h/R \leqslant 2$ are found to be

$$d_1\left(\frac{h}{R}\right) = -5.90 + 13.31\left(\frac{h}{R}\right) - 14.54\left(\frac{h}{R}\right)^2 + 7.31\left(\frac{h}{R}\right)^3 - 1.35\left(\frac{h}{R}\right)^4, \tag{26}$$

$$d_2\left(\frac{h}{R}\right) = 33.43 - 117.59\left(\frac{h}{R}\right) + 152.05\left(\frac{h}{R}\right)^2 - 81.73\left(\frac{h}{R}\right)^3 + 15.49\left(\frac{h}{R}\right)^4, \tag{27}$$

$$d_3\left(\frac{h}{R}\right) = -96.60 + 357.34\left(\frac{h}{R}\right) - 479.04\left(\frac{h}{R}\right)^2 + 263.04\left(\frac{h}{R}\right)^3 - 50.44\left(\frac{h}{R}\right)^4, \tag{28}$$

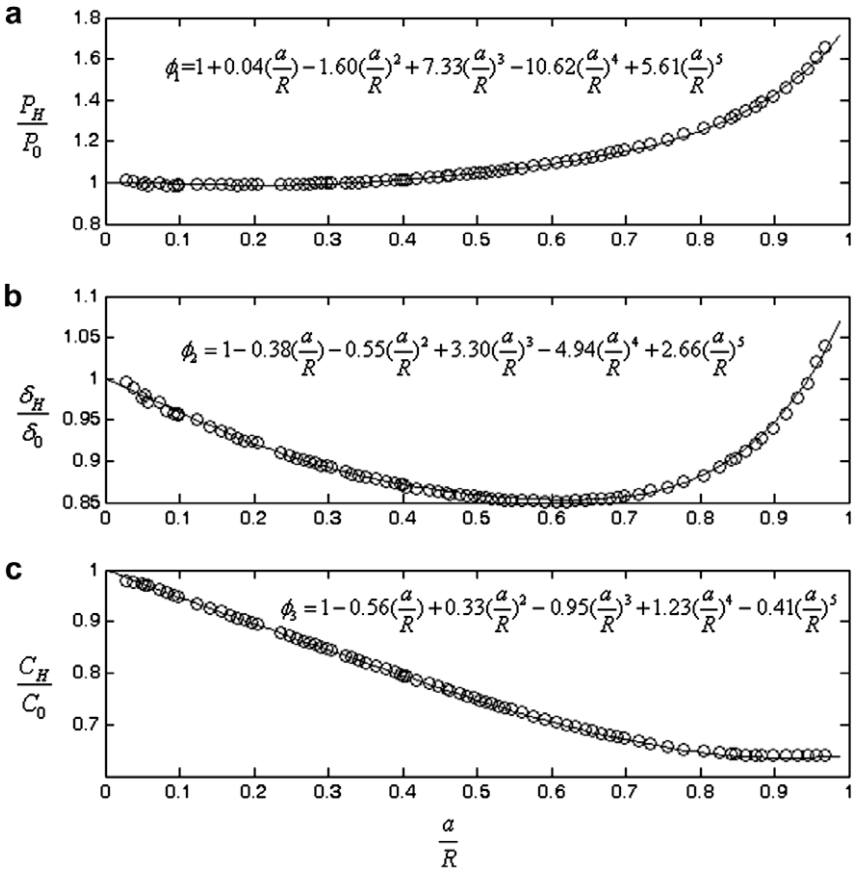

Fig. 7. For $h/R = 1.8$, (a) FEM results (○) of P_H/P_o versus a/R and its fitting function ϕ_1 (solid line) (b) FEM results (○) of δ_H/δ_o versus a/R and its fitting function ϕ_2 (solid line) (c) FEM results (○) of C_H/C_o versus a/R and its fitting function ϕ_3 (solid line).

$$d_4\left(\frac{h}{R}\right) = 136.38 - 490.07\left(\frac{h}{R}\right) + 651.96\left(\frac{h}{R}\right)^2 - 357.42\left(\frac{h}{R}\right)^3 + 68.5\left(\frac{h}{R}\right)^4, \tag{29}$$

$$d_5\left(\frac{h}{R}\right) = -66.21 + 231.12\left(\frac{h}{R}\right) - 304.47\left(\frac{h}{R}\right)^2 + 166.48\left(\frac{h}{R}\right)^3 - 31.87\left(\frac{h}{R}\right)^4. \tag{30}$$

6. Results of adhesive contact and comparison

The relation between load and projected contact radius for the adhesive contact of a spherical rigid indenter and the Neo-Hookean layer is obtained using (6) and the results of the last section. Specifically, the load versus contact radius for large-deformation JKR theory can be calculated by

$$P = P_o\phi_1\left(\frac{a}{R},\frac{h}{R}\right) - \sqrt{\frac{-4\pi aW\left[1-\left(\frac{a}{R}\right)^2\right]^{-1/2}}{C_o'\phi_3\left(\frac{a}{R},\frac{h}{R}\right)+C_o\phi_3'\left(\frac{a}{R},\frac{h}{R}\right)}}, \tag{31}$$

where the prime denotes d/da. Similarly, using (5) and the large-deformation Hertz displacement δ_H and compliance C_H given above, the relation between the displacement and the contact radius in the large-deformation JKR theory is

$$\delta = \delta_o\phi_2\left(\frac{a}{R}\right) - C_o\phi_3\left(\frac{a}{R}\right)\sqrt{\frac{-4\pi aW\left[1-\left(\frac{a}{R}\right)^2\right]^{-1/2}}{C_o'\phi_3\left(\frac{a}{R}\right)+C_o\phi_3'\left(\frac{a}{R}\right)}}. \tag{32}$$

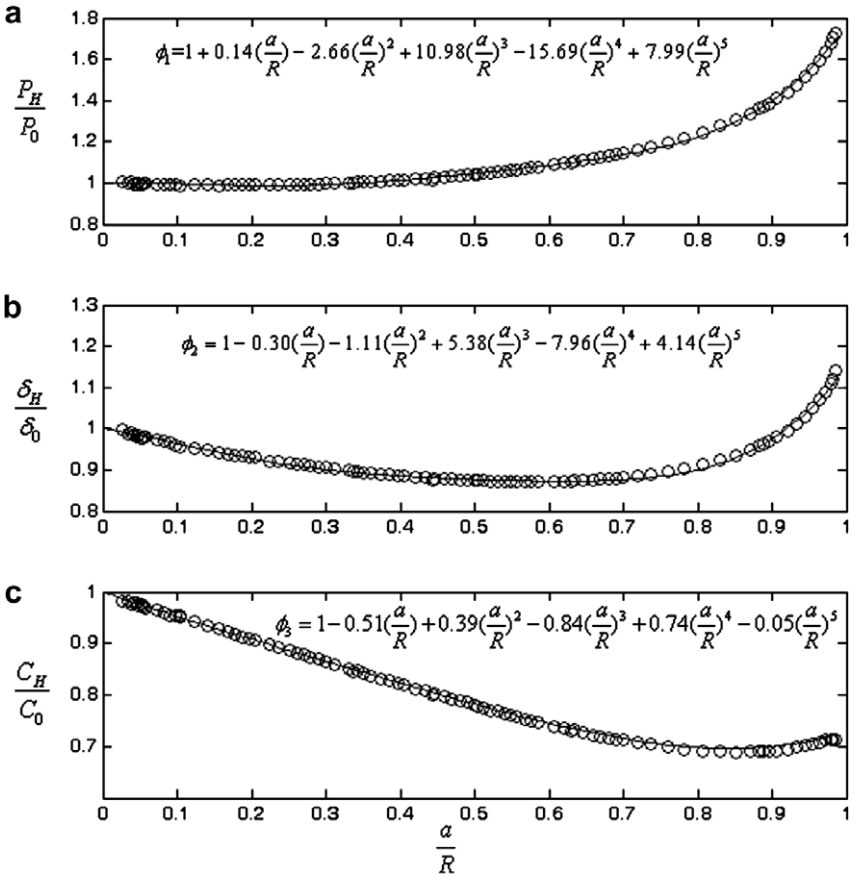

Fig. 8. For $h/R = 2.0$, (a) FEM results (○) of P_H/P_o versus a/R and its fitting function ϕ_1 (solid line) (b) FEM results (○) of δ_H/δ_o versus a/R and its fitting function ϕ_2 (solid line) (c) FEM results (○) of C_H/C_o versus a/R and its fitting function ϕ_3 (solid line).

The theory used to obtain (31) and (32) is exact except for the approximation used to derive Eqs. (5) and (6). The accuracy of this assumption as well as the accuracy of our fits to finite element results has been checked by separate finite element analyses to directly simulate the adhesive contact between a spherical indenter and the elastic layer. In the direct finite element simulation of adhesive contact, the adhesive forces between two contacting surfaces were modeled by the cohesive zone model, which has been used to study the interfacial forces between solids by many investigators (Barthel, 1998; Jagota et al., 1998; Lin and Hui, 2002). Excellent agreement between our theory and direct finite element solution using the cohesive zone model (Dugdale–Barenblatt model (Dugdale, 1960; Barenblatt, 1968)) was obtained for a spherical indenter contacting on a layer with thickness $h = 10R$ and has shown in Lin and Chen (2006). The reasoning is as follows: for small contact, the assumption (2) holds because linear theory is a good approximation, and for large contact, the actual displacement is very close to the large-deformation Hertz displacement. That is, $\delta - \delta_H$ is indeed very small in comparison with δ_H.

To take into account of the work of adhesion and compare our results with the JKR theory, we introduce the following normalized variables:

$$\overline{A} = \frac{a}{\left[\frac{3\pi W R^2}{16\mu}\right]^{\frac{1}{3}}}, \tag{33}$$

$$\overline{P} = \frac{P}{\pi W R}, \tag{34}$$

$$\bar{\delta} = \frac{\delta}{\left[\frac{9\pi^2 W^2 R}{256\mu^2}\right]^{\frac{1}{3}}}, \tag{35}$$

where $\overline{A}, \overline{P}, \bar{\delta}$ are the normalized contact radius, normalized load and normalized displacement, respectively. The normalized contact radius, a/R in the previous section is related to the new normalized contact radius by

$$\frac{a}{R} = \beta\overline{A}, \quad \text{where } \beta = \left(\frac{3\pi W}{16\mu R}\right)^{1/3}. \tag{36}$$

Detailed calculations of Eqs. (31) and (32) using normalizations (33)–(36) were given in Appendix A. Figs. 9 and 10 show the predictions of $\overline{P}$ and $\bar{\delta}$ at a fixed normalized contact radius $\overline{A}$ by (A3) and (A4) for various layer thickness h, respectively. Also shown in Figs. 9 and 10 are predictions based on the small strain JKR theory (solid lines) as comparison. The equations of the small strain JKR theory, in normalized form, are

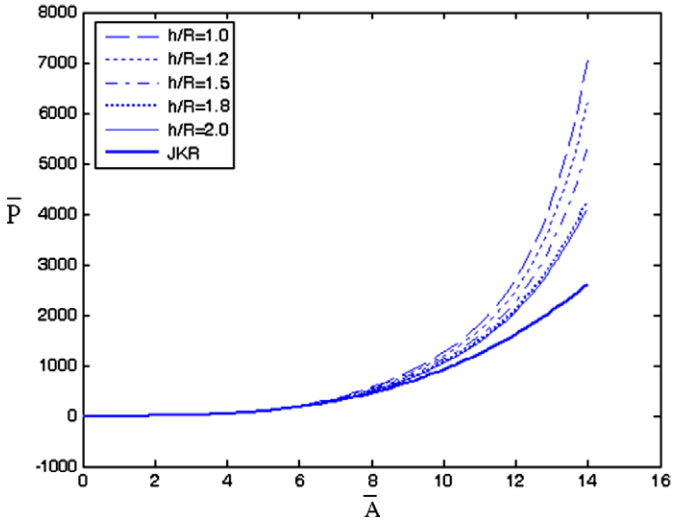

Fig. 9. Comparison of normalized load $\overline{P}$ versus normalized contact radius $\overline{A}$ curves predicted by our theory for different layer thickness. The prediction by JKR theory is plotted as comparison.

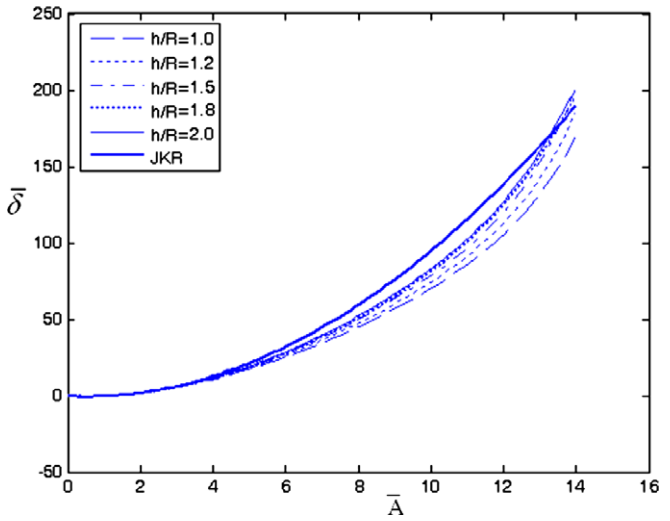

Fig. 10. Comparison of normalized displacement $\bar{\delta}$ versus normalized contact radius $\overline{A}$ curves predicted by our theory for different layer thickness. The prediction by JKR theory is plotted as comparison.

$$\overline{P} = \overline{A}^3 - \sqrt{6\overline{A}^3}, \tag{37}$$

$$\bar{\delta} = \overline{A}^2 - \frac{2}{3}\sqrt{6\overline{A}}. \tag{38}$$

The parameters used for the normalization are $W = 0.06\ \mathrm{J/m^2}$, $R = 10\ \mu\mathrm{m}$, $\mu = 10\ \mathrm{MPa}$, so that $\beta = 0.0707$.

7. Conclusion and discussion

Based on our numerical results, we obtain analytic expressions which relate the applied load or applied displacements to the contact radius and the work of adhesion in the large-deformation regime. These expressions are given by (31) and (32). When the contact area is very small, these expressions reduce to the standard small strain JKR theory.

For non-adhesive contact of a rigid indenter with radius R and hyperelastic layers with thickness h and $1 \leqslant h/R \leqslant 2$, our results show that for small to medium contact, the load versus contact radius relation predicted by the small strain Hertz theory is quite accurate. For contact radius exceeding 40% of the indenter radius, the small strain JKR theory can considerably underestimates the actual load. On the other hand, the relationship between displacement and contact radius differs from the small strain theory except for extremely small contact. However, the difference is less than 25% for $a/R < 1$. Our results show that the differences between the two theories do not always increase with contact radius, especially for thin layers. The same trends are observed for adhesive contact. In light of this, if JKR theory was to be used to interpret experimental data, then the force versus contact area relation should be used for small to moderate deformation while the displacement versus contact radius relation should be used for very large deformation.

Also, to give a sense of what the deformation pattern looks like at large a/R, the deformed configuration obtained from the FEM result of a hyperelastic layer of $h/R = 1.0$ and $a/R = 0.98$ is shown in Fig. 11.

Our results can be easily modified to model adhesion hysteresis due to rate processes on the interface, such as the formation and breaking of hydrogen bonds (Ghatak et al., 2000). The only restriction is: (1) the region where the interfacial rate processes occurs is very small in comparison with the contact area, so that the processes are completely controlled by the energy release rate computed based on elasticity theory; (2) the bulk material is hyperelastic. For these cases, the work of adhesion in Eqs. (31) and (32) must be regarded as history dependent quantities; reflecting the fact that interfacial fracture is rate dependent.

There are several limitations in this work. Our computations are carried out using a Neo-Hookean solid whereas the behavior of soft materials can be substantially different from this idealized model, especially at

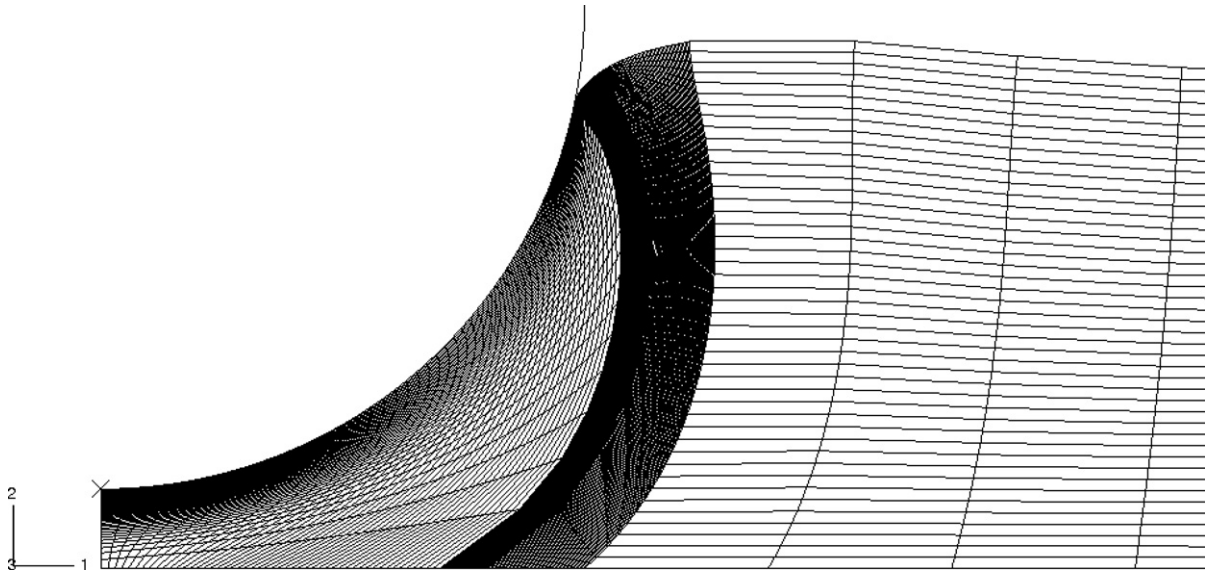

Fig. 11. The deformed configuration of the hyperelastic layer of $h/R = 1.0$ at $a/R = 0.98$.

very large deformation. For example, Kawamura et al. (2001) and Urayama et al. (2001) have shown that the strain energy density function of poly(dimethylsiloxane) (PDMS) networks under multi-axial loading deviates significantly from that of a Neo-Hookean solid. However, it should be noted that the validity of the theory presented in this work is independent of the form of the strain energy density function, as long as the material is hyperelastic. Instead of using a strain energy density function which works well for a particular elastomer, we have chosen to carry out our calculations on an idealized model which has universal appeal. There is no difficulty using the same procedures shown in this work to study the adhesive contact mechanics of any hyperelastic solid, irrespective of the form of strain energy density function. Finally, we have used frictionless boundary condition on the contacting interface. This is a standard assumption in contact mechanics. Undoubtedly our results will change if no sliding is permitted on the interface, especially when the contact radius is large. We do not expect this change will be very significant, since the bottom of the layer is perfectly bonded to a rigid layer.

Acknowledgements

The authors wish to thank for Dr. P. Cole for bring the problem first to our attention. They also want to thank Dr. C.Y. Hui for fruitful discussions. This work was supported by National Science Council (95-2211-E-006-465) in Taiwan.

Appendix A

Using normalization of (33)–(36), (31) and (32) can be rewritten as

$$\overline{P} = \overline{A}^3\phi_1 - \sqrt{\frac{6\overline{A}^3(1-\beta^2\overline{A}^2)^{-1/2}}{\phi_3(\beta\overline{A}) - \beta\overline{A}\phi_3'(\beta\overline{A})}} \tag{A1}$$

and

$$\bar{\delta} = \overline{A}^2\phi_2 - \frac{2\phi_3}{3\overline{A}}\sqrt{\frac{6\overline{A}^3(1-\beta^2\overline{A}^2)^{-1/2}}{\phi_3(\beta\overline{A}) - \beta\overline{A}\phi_3'(\beta\overline{A})}}, \tag{A2}$$

respectively, where the prime denotes $\mathrm{d}/\mathrm{d}(\beta\overline{A})$. Substituting (27)–(29) into A1 and A2, the normalized load $\overline{P}$ and the normalized displacement $\bar{\delta}$ for adhesive contact between a hyperelastic hemisphere and a rigid substrate are given by

$$\overline{P} = \overline{A}^3(1 + b_1\beta\overline{A} + b_2\beta^2\overline{A}^2 + b_3\beta^3\overline{A}^3 + b_4\beta^4\overline{A}^4 + b_5\beta^5\overline{A}^5) - \sqrt{\frac{6\overline{A}^3(1-\beta^2\overline{A}^2)^{-1/2}}{1 - d_2\beta^2\overline{A}^2 - 2d_3\beta^3\overline{A}^3 - 3d_4\beta^4\overline{A}^4 - 4d_5\beta^4\overline{A}^4}} \tag{A3}$$

and

$$\bar{\delta} = \overline{A}^2(1 + c_1\beta\overline{A} + c_2\beta^2\overline{A}^2 + c_3\beta^3\overline{A}^3 + c_4\beta^4\overline{A}^4 + c_5\beta^5\overline{A}^5) - \frac{2}{3}(1 + d_1\beta\overline{A} + d_2\beta^2\overline{A}^2 + d_3\beta^3\overline{A}^3 + d_4\beta^4\overline{A}^4 + d_5\beta^5\overline{A}^5) \times \sqrt{\frac{6\overline{A}(1-\beta^2\overline{A}^2)^{-1/2}}{1 - d_2\beta^2\overline{A}^2 - 2d_3\beta^3\overline{A}^3 - 3d_4\beta^4\overline{A}^4 - 4d_5\beta^4\overline{A}^4}}, \tag{A4}$$

respectively.

References

Ahn, D., Shull, K.R., 1998. Effects of methylation and neutralization of carboxylated poly(*n*-butyl acrylate) on the interfacial and bulk contributions to adhesion. Langmuir 14 (13), 3637–3645.

Barenblatt, G.I., 1968. Mathematical theory of equilibrium cracks in brittle fracture. Advances in Applied Mechanics 7, 55–129.

Barthel, E., 1998. On the description of the adhesive contact of spheres with arbitrary interaction potentials. Journal of Colloid and Interface Science 200 (1), 7–18.

Barthel, E., Parriot, A., 2007. Adhesive contact to a coated elastic substrate. Journal of Physics D – Applied Physics 40 (4), 1059–1067.

Chaudhury, M.K., Whitesides, G.M., 1991. Direct measurement of interfacial interactions between semispherical lenses and flat sheets of poly(dimethylsiloxane) and their chemical derivatives. Langmuir 7 (5), 1013–1025.

Dugdale, D.S., 1960. Yielding of steel sheets containing slits. Journal of the Mechanics and Physics of Solids 8, 100–104.

Ghatak, A., Vorvolakos, K., She, H.Q., Chaudhury, M.K., 2000. Interfacial rate processes in adhesion and friction. Journal of Physical Chemistry B 104 (17), 4018–4030.

Hui, C.Y., Lin, Y.Y., Baney, J.M., Jagota, J., 2000. The accuracy of the geometric assumptions in the JKR (Johnson–Kendall–Roberts) theory of adhesion. Journal of Adhesion Science and Technology 14 (10), 1297–1319.

Jagota, A., Argento, C., Mazur, S., 1998. Growth of adhesive contacts for Maxwell viscoelastic spheres. Journal of Applied Physics 83, 250–259.

Johnson, K.L., Kendall, K., Roberts, A.D., 1971. Surface energy and the contact of elastic solids. Proceedings of the Royal Society A – Mathematical Physical and Engineering Science 324, 301–313.

Kawamura, T., Urayama, K., Kohji, S., 2001. Multiaxial deformations of end-linked poly(dimethylsiloxane) networks. 1. Phenomenological approach to strain energy density function. Macromolecules 34 (23), 8252–8260.

Lin, Y.Y., Hui, C.Y., 2002. Mechanics of contact and adhesion between viscoelastic spheres: an analysis of hysteresis during loading and unloading. Journal of Polymer Science Part B: Polymer Physics 40 (9), 772–793.

Lin, Y.Y., Chen, H.Y., 2006. Effect of large deformation and material nonlinearity on the JKR (Johnson–Kendall–Roberts) test of soft elastic materials. Journal of Polymer Science Part B: Polymer Physics 44 (19), 2912–2922.

Maugis, D., Barquins, M., 1978. Fracture mechanics and the adherence of viscoelastic bodies. Journal of Physics D – Applied Physics 11, 1989–2023.

Reedy, E.D., 2006. Thin-coating contact mechanics with adhesion. Journal of Material Research 21 (10), 2660–2668.

Shull, K.R., Ahn, D., Chen, W.L., Flanigan, C.M., Crosby, A.J., 1998. Axisymmetric adhesion tests of soft materials. Macromolecular Chemistry and Physics 199 (4), 489–511.

Shull, K.R., 2002. Contact mechanics and the adhesion of soft solids. Materials Science & Engineering R – Reports 36 (1), 1–45.

Urayama, K., Kawamura, T., Kohji, S., 2001. Multiaxial deformations of end-linked poly(dimethylsiloxane) networks. 2. Experimental tests of molecular entanglement models of rubber elasticity. Macromolecules 34 (23), 8261–8269.

Yang, F.Q., 2003a. Thickness effect on the indentation of an elastic layer. Materials Science & Engineering A – Structural Material Properties Microstructure and Processing 358 (1–2), 226–232.

Yang, F.Q., 2003b. Adhesive contact of axisymmetric suspended miniature structure. Sensors and Actuators A – Physical 104 (1), 44–52.